Research Article | Vol. 33, No. 8 / 21 Apr 2025 / Optics Express 17192

Optics EXPRESS

Narrow linewidth III-V-on-SiN laser with extended frequency chirp capability based on micro-transfer printing for high resolution distributed acoustic sensing

G. Dandé,[1,2,*] J. Pennanech,[1] C. Charliac,[1] V. Kemlin,[1] V. Crozatier,[1] I. Ghorbel,[1] V. Billault,[1] B. Pan,[3] E. Soltanian,[3] J. Zhang,[3] G. Roelkens,[3] M. Dahlem,[4] J. Song,[4] S. Dwivedi,[4,5] D. Carbajal Altamirano,[4] C. Cummins,[4] S. Seema Saseendran,[4] P. Helin,[4] J. Ramirez,[6] D. Néel,[6] H. Guillet De Chatellus,[2] and J. Bourderionnet[1]

[1] *Thales Research and Technology, 1 Avenue Augustin Fresnel, Palaiseau 91767, France*
[2] *Univ Rennes, CNRS, Institut FOTON- UMR 6082, 35000 Rennes, France*
[3] *Photonics Research Group, Department of Information Technology (INTEC), Ghent University - IMEC, Ghent 9052, Belgium*
[4] *IMEC, Kapeldreef 75, Heverlee 3001, Belgium*
[5] *Texas Instruments Inc., Leonardo Da Vincilaan 19, 1831 Diegem, Belgium*
[6] *III-V Lab, 1 Avenue Augustin Fresnel, Palaiseau 91767, France*
[*] *guenole.dande@thalesgroup.com*

Abstract: A laser source that is both narrow-linewidth and frequency-agile is essential for FMCW applications, such as LIDAR or distributed optical fiber sensing (DOFS). In this work, we present the design and characterization of a laser architecture based on the heterogeneous integration of III-V gain material on a SiN photonic circuit that meets these specifications. By incorporating a dual-ring resonator mirror in the cavity, we achieved a linewidth of 2.4 kHz and a large frequency excursion. We obtained chirps with an amplitude of 20 GHz, with residual nonlinearities of less than 1%. A preliminary DOFS measurement was carried out, demonstrating the excellent performance of the laser.

© 2025 Optica Publishing Group under the terms of the Optica Open Access Publishing Agreement

1. Introduction

Distributed optical fiber sensors (DOFS) are one of the most promising technologies in the sensor industry. With an ever-expanding range of applications since their emergence in the late '80s, they can now be found in many fields [1], from bio-chemistry to infrastructure monitoring [2] and seismology [3]. Their principle relies on the sensitivity of optical fibers to their environment, enabling them to quantify physical quantities such as temperature, pressure or strain. In addition to interacting with the transmitted optical signal, all these quantities will also affect the backscattered light along the fiber. Rayleigh backscattering is commonly used in DOFS applications [4]. It is caused by impurities naturally present in the fiber, which are very small compared to the propagating telecom wavelength. Thanks to the random distribution of these scatterers, the light is back-reflected all along the fiber, enabling the latter to be used for distributed sensing. The backscattered signal can be analyzed at the fiber input using two distinct methods [5]: OTDR (optical time domain reflectometry) and OFDR (optical frequency domain reflectometry). OFDR is based on an approach similar to the FMCW (frequency modulated continuous wave) technique used in radar and lidar [6]. Unlike OTDR, where position mapping is performed in the time

#529238 https://doi.org/10.1364/OE.529238
Journal © 2025 Received 30 May 2024; revised 9 Aug 2024; accepted 16 Sep 2024; published 10 Apr 2025

Optics EXPRESS

domain, OFDR techniques transpose position in frequency domain. The principle of OFDR is illustrated in Fig. 1. A CW laser source with linearly swept frequency probes the device under test (DUT) interferometer. The first arm (1) of the interferometer includes a circulator to interrogate the fiber under test (FUT) and recover the backscattered signal. The second arm (2) acts solely as a local oscillator. When the two arms are recombined on a detector, the reflectivity profile in the FUT is mapped into the electrical spectrum of the photodetection signal. The laser source frequency ramp waveform is defined by the laser modulation period (T_{mod}), the chirp amplitude (Δf) and its chirp linearity. An auxiliary interferometer is commonly used to calibrate the frequency modulation and thus better compensate for chirp nonlinearities by post-processing or pre-compensation.

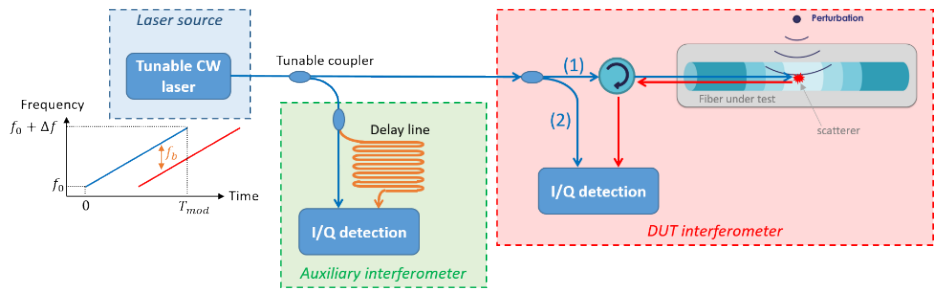

Fig. 1. OFDR interrogator schematic diagram.

To demodulate an OFDR signal, two steps are required. First, we consider a sample of the electrical beat signal of duration T_{mod}, on which we perform a Fourier transform. The environment of the fiber affects the amplitude and/or phase of the beatnotes. The second step consists in linking the frequency domain to the spatial domain, according to the following relation:

$$f_b = \gamma.\tau = \gamma.\frac{2.n_{eff}.z}{c} \tag{1}$$

with $\gamma = \Delta f / T_{mod}$ the frequency sweeping rate, n_{eff} the effective index of the FUT and z the distance from the scattering center, c is the light velocity in vacuum. The sensor's theoretical spatial resolution ($\Delta z_{\min}$), which corresponds to the minimum distance that can be resolved between two scattering centers, is thus directly linked to the frequency resolution of the Fourier transform. In FMCW, the theoretical spectral resolution of the Fourier Transform is equal to the inverse of the sample duration $1/T_{mod}$ (temporal windowing), leading to the following equation:

$$\Delta f_{b,min} = \frac{1}{T_{mod}} \Rightarrow \Delta z_{\min} = \frac{c}{2.n_{eff}.\Delta f} \tag{2}$$

As a result, the spatial resolution of the sensor is directly proportional to the inverse of the chirp amplitude. Assuming that an OFDR spectrum is acquired every T_{mod}, the sensor's detection bandwidth B_W is thus equal to $[0,\ 1/2T_{mod}]$ to meet Shannon's criterion. Additionally, the optical phase noise of the laser affects the noise floor of the measurement. Therefore, it is crucial to use a narrow linewidth laser, in particular for long interrogation distances. In summary, DOFS performance is extremely dependent on the laser source used for an OFDR-type approach. Among the semiconductor lasers, DBR lasers [7] have the advantage of being compact and can produce chirps of several tens of GHz, corresponding to sub-cm spatial resolution. However, their wide linewidth (>100 kHz) significantly degrades the noise floor of the measurement and limits their use. Alternatively, recent advances in low-loss materials such as silicon or silicon nitride have led to the development of high-quality ring resonators that drastically improve the laser linewidth

Optics EXPRESS

when using an external cavity geometry. These rings can be placed directly in the laser cavity by hybrid [8] or heterogeneous [9] integration with a III-V material, thus narrowing the linewidth below ten kHz or even sub kHz. They can also be used together with a DFB for self-injection locking to achieve linewidths of a few tens of Hz [10]. However, the use of ring resonators limits the chirp amplitude to the filter bandwidth. Therefore, simultaneous modulation of the filter and longitudinal modes is required to achieve large chirp amplitude. Frequency modulation on SiN resonators can be achieved either by inverse piezoelectric effect or by thermo-optic effect. The former enables fast modulation (>100 kHz) but with limited efficiency (a few GHz), while the latter enables large excursions (several tens of GHz) but with a modulation frequency of no more than 10 kHz.

Finally, the architecture of a DOFS is not limited solely to that of its laser, and the ultimate goal of this work is to develop a complete architecture that integrates not only the laser, but also the interferometer and the photodetector. This is one major interest of the platform presented in this paper, which combines the ultra-low losses of SiN with the active functionality of InP through micro-transfer printing (µTP). µTP is a promising heterogeneous integration process that enables different materials to be combined on the same platform, in a scalable fashion. To achieve this, coupons of III-V SOAs are transferred onto a SiN wafer [11]. In this paper, we present in detail the design and characterization of an FMCW laser source based on the heterogeneous integration of III-V material on SiN. Using a dual ring-resonators mirror, we obtained a narrow laser linewidth (2.4 kHz) and chirp excursions >20 GHz. This performance made it possible to realize a first dynamic OFDR measurement, demonstrating the high potential of the realized architecture and the platform for DOFS applications.

2. Tunable laser source

The laser circuit design layout is shown in Fig. 2, with its four main constitutive building blocks, namely (a) the tunable output coupler, (b) the gain section, (c) the phase section and (d) the frequency selective back mirror. The passive sections (building blocks (a), (c) and (d)) are realized on a SiN circuit, while the active section (b) is realized on an InP SOA coupon before being transferred to the SiN platform [11]. In order to overcome the significant refractive index mismatch between SiN and InP, a two-stage adiabatic structure with an a-Si:H waveguide interlayer has been developed. This allows a good coupling efficiency to be achieved [12]. Details of the platform and fabrication process steps can be found in [13].

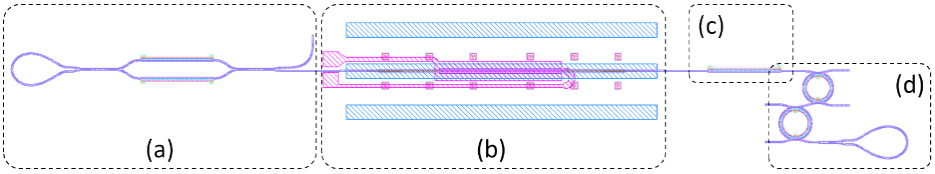

Fig. 2. Laser cavity design. (a) Front mirror, (b) gain medium, (c) phase section, (d) frequency selective back mirror.

The front mirror (a) is built on a Sagnac loop mirror closed by a Mach-Zehnder interferometer with 500µm-length thermo-optic phase shifters on both arms. Applying a voltage to the phase shifters then allows to modify the ratio between the optical intensity exiting the laser cavity and the intensity back-reflected to the gain medium. Typically, the mirror is set to 50% reflectivity to optimize laser output. The laser cavity gain medium (b) is based on an InGaAlAs/InGaAs multi-quantum wells (MQW) structure. The phase section (c) is a 500 µm length thermo-optic phase shifter, used to align the laser cavity modes with the intracavity filter central frequency. The frequency selective back mirror (d) is composed of two cascaded add-drop ring resonator

Optics EXPRESS

filters followed by a Sagnac loop mirror. The design of this last block is the most important for the laser performances.

2.1. Design of the frequency selective mirror

Inserting a ring resonator mirror in the cavity has three objectives: high reflectivity, wavelength selectivity (to ensure the laser's single-mode behavior) and linewidth enhancement. The Sagnac loop ensures reflectivity, while frequency filtering is based on the Vernier effect obtained by cascading two ring resonators of slightly different diameters in an add-drop configuration. The transmission of each ring and the resulting transmission of this combination are shown in Fig. 3(a).

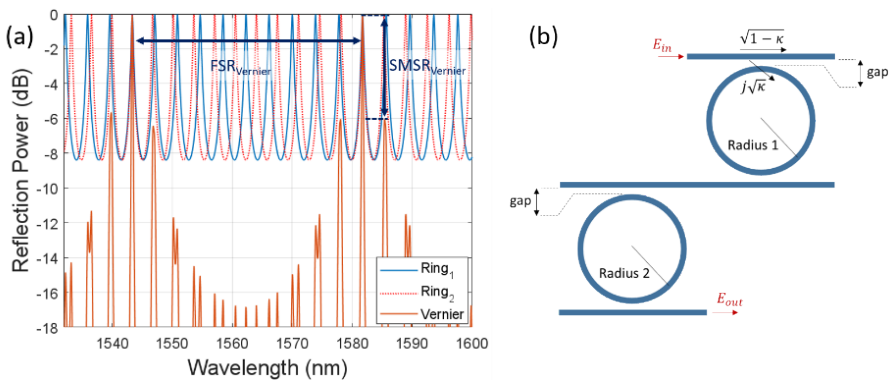

Fig. 3. (a) Schematic of the optical transmission of the individual rings (blue and red), and optical transmission of the cascaded rings (Vernier effect). (b) Definition and design parameters of the Vernier filter.

To design the filter, three parameters need to be defined: the radius of the smaller ring (r_1), the radius of the larger one ($r_2 = r_1 + \Delta R$) and the coupling of the ring to the waveguide (κ). The latter depends on the gap between them, set identical for the two rings.

To tune the filter (i.e., the lasing frequency), the free spectral range (FSR) of the rings is adjusted using the thermo-optic effect. The smallest ring radius is set to 100 µm, large enough to allow the 2π phase shift required for a complete tunability of the laser within the current acceptance of the heaters. Then we set the difference between the radii (ΔR). Figure 3(a) shows that the reflection maximum occurs when the wavelength satisfies the resonance condition of the two rings. The $FSR_{Vernier}$ resulting from the combination of two ring resonators is given by the following equation [14].

$$FSR_{Vernier} = \frac{FSR_1.FSR_2}{|FSR_1 - FSR_2|} \tag{3}$$

with $FSR_n = \lambda^2/2\pi.R_n.n_g$ the FSR of the resonator n. The lower ΔR, the higher the equivalent FSR. The advantage of a high $FSR_{Vernier}$ is to increase the laser's tuning range by ensuring its single-mode behavior over a wide bandwidth. Typically, $FSR_{Vernier}$>25 nm is sufficient to maintain single-mode operation, which corresponds to a radius difference of less than 7.5 µm. On the other hand, if ΔR is too low, the filter's side mode suppression ratio (SMSR) decreases, as shown in Fig. 4(a). Therefore a first trade-off has to be found between the filter's SMSR and its FSR. Moreover, the filter's SMSR also depends on the coupling coefficient κ of the resonators.

The latter depends on the gap between the waveguide and the ring (see Fig. 3(b)). This coefficient is important in design optimization, as it determines the loaded quality factor (Q-factor) of the resonator, which affects the frequency selectivity of the ring and the laser linewidth. The loaded Q-factor can be defined as the ratio between the filter's center wavelength and the resonance's full width at half maximum (FWHM) [15]. In other words, a high Q-factor will give

Optics EXPRESS

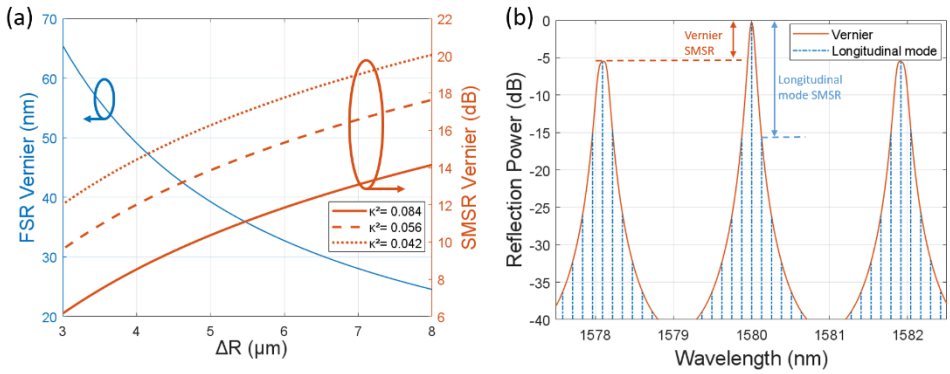

Fig. 4. (a) Simulated Vernier FSR (left axis) and Vernier SMSR (right axis) for different values of the ring coupling ratio κ as a function of ΔR. (b) Illustration of the side mode suppression ratio (SMSR) of the Vernier filter.

a better rejection of the Vernier filter modes, and also of the laser longitudinal modes, thanks to a narrower filter resonance (see Fig. 4(b)). A SMSR of 10 to 15 dB is sufficient to guarantee the laser's single-mode behavior. However, if the coupling is too weak (i.e., Q-Factor too high), the filter insertion loss can increase due to the waveguide propagation loss. There is therefore a second compromise to be found in order to combine a sufficient SMSR with the lowest insertion loss. Considering propagation losses between 5 dB/m and 25 dB/m in the worst-case scenario limits the loaded quality factor to below 60,000.

2.2. Laser linewidth

In DOFS applications, the laser's linewidth is a crucial parameter for interrogating long fiber distances with a low noise floor, requiring the use of high-quality ring resonators in the cavity. In particular, the multiple turns performed in each of the rings extend the length of the cavity, leading to a reduction in the laser's linewidth. According to the formalism used by Kazarinov and Henry [16], when the cavity is coupled with a resonator, the Lorenztian linewidth of a semiconductor laser ($\Delta\nu_{ST}$) is reduced by a factor $F^2 = (1 + A + B)^2$, where:

$$\Delta\nu = \frac{\Delta\nu_{ST}}{F^2} \tag{4}$$

$$A = \frac{1}{\tau_0} \cdot \frac{d\phi_{eff}(\omega)}{d\omega} \tag{5}$$

$$B = \frac{\alpha_H}{\tau_0} \cdot \frac{d\ln(|r_{eff}(\omega)|)}{d\omega} \tag{6}$$

with τ_0 the round-trip time of a photon in the active section, α_H the linewidth enhancement factor, $\phi_{eff}(\omega)$ and $|r_{eff}(\omega)|$ the respective phase and amplitude terms of the complex reflectivity of the mirror. Figure 5(c) illustrates the relationship between the loaded Q-Factor and the linewidth reduction factor F^2 as a function of the coupling between the ring and the waveguide. In order to meet the requirements of DOFS applications, a linewidth below 10 kHz is expected. Given that the linewidth of a semiconductor laser without high-Q cavities is a few MHz, a reduction in laser linewidth of a few 100 to 1000 times is required, corresponding to a loaded Q-factor between 30,000 and 60,000. To observe the effect of the quality factor on laser linewidth, we studied two laser designs. The first laser has a fixed gap between ring and bus waveguide of 0.5 μm, resulting in a loaded quality factor of 30,000, while the second laser has a fixed gap of 0.6 μm,

Optics EXPRESS

resulting in a loaded quality factor of 60,000. The ring radii are fixed at 100 µm and 105.96 µm for both lasers. Figure 5(a) presents the spectrum obtained from the through port of the smallest ring, with a radius of 100 µm, in the two laser configurations studied. The experimental loaded Q-Factor values of 38 k and 57 k were deduced from the full-width at half-maximum (FWHM) of the notch, which aligns with the expected values of 30 k and 60 k, respectively. These high quality factors enabled single-mode operation on both lasers with side-mode suppression ratio (SMSR) values of 57 dB and 60 dB respectively (Fig. 5(b)).

Figure 5(d) displays the optical frequency noise measured at an input power of 0.25 mW for both lasers using the self-heterodyne method with a 50 m delay line [16,17]. From the white noise floor (f_w) we extract the Lorentzian linewidth $\Delta\nu = \pi.f_w$. The laser with a filter loaded Q-factor of 30,000 has a linewidth of 9.9 kHz, while the laser with a filter loaded Q-factor of 60,000 has a linewidth of 2.4 kHz. These results are in excellent agreement with the simulated F^2 reduction factor for the two different coupling coefficients (1/244 for 30,000 and 1/898 for 60,000 Q-factor).

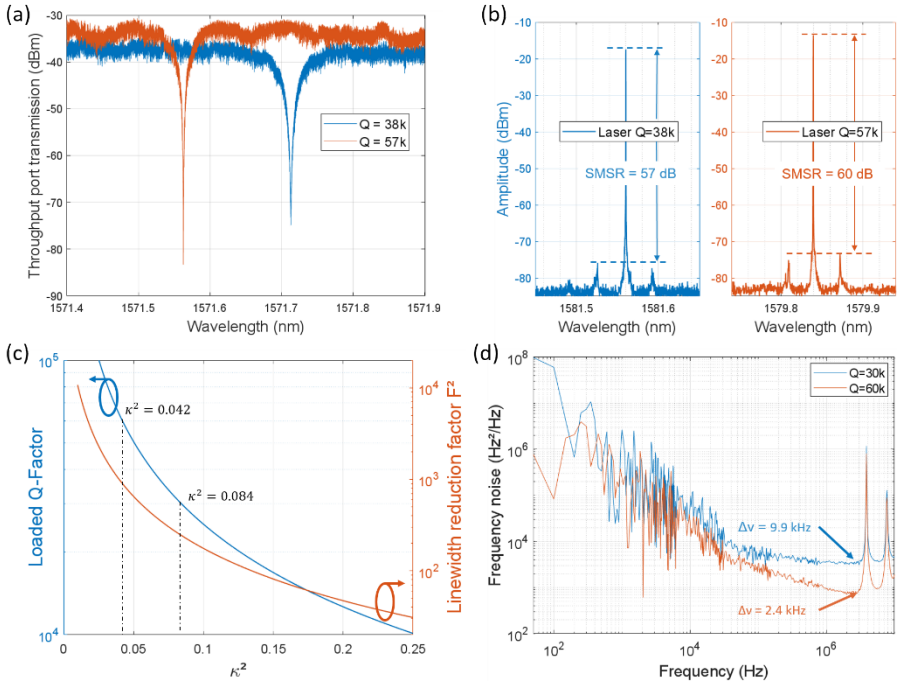

Fig. 5. (a) Transmission spectrum obtained on the through port of MRRs with a radius of 100 µm for a gap of 0.5 µm (blue) and 0.6 µm (orange). (b) Optical spectrum for the two different lasers studied. (c) Linewidth reduction factor F^2 and corresponding filter loaded Q-factor as a function of the rings coupling coefficient κ. Values for the limits κ=0.042 and κ=0.084 are indicated with arrows (loaded Q = 60,000 and 30,000 respectively). (d) Frequency noise spectrum for the two different lasers studied

For a DOFS application, it is necessary to maintain the linewidth constant during the chirp. Therefore, we investigated its evolution as a function of frequency detuning. The minimum linewidth is obtained for a slightly negative detuning from the filter central frequency, where F^2 is at its maximum. This phenomenon is linked to the B coefficient of Eq. (6), which describes a process of laser frequency stabilization by negative feedback effect [9] when $dr_{eff}(\omega)/d\omega>0$. The B factor therefore reaches a maximum when the laser frequency is slightly lower than that of the filter's reflection maximum. We verified experimentally this phenomenon by varying the

Optics EXPRESS

phase in the cavity to slightly modify the laser frequency. Figure 6 shows the experimental and simulated results of linewidth evolution as a function of frequency detuning for the two laser configurations studied. The blue dots show the laser output power.

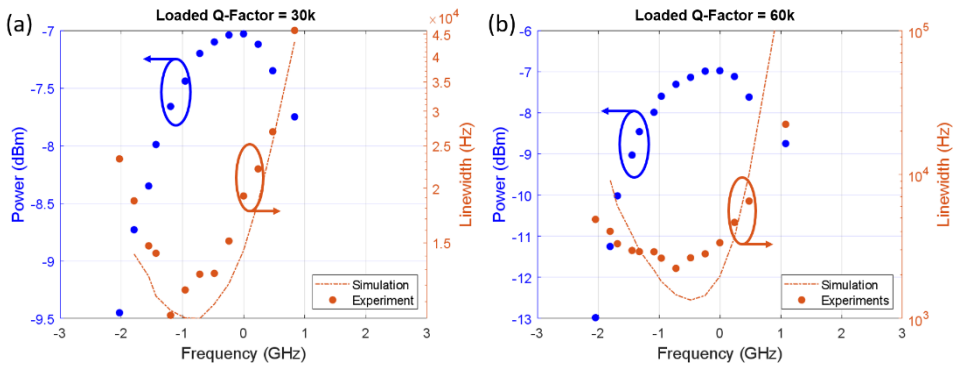

Fig. 6. Laser output power and the extracted linewidth from frequency noise measurement as a function of the detuned frequency for the two architectures studied (a) Q = 30,000 and (b) Q = 60,000. The solid line shows the theoretical curve calculated from Eq. (4) with $\alpha_H = 2.5$ and the experimentally measured output power.

We observe a good agreement between the measurements and the simulation for both lasers. Additionally, the influence of coefficient B is evidenced, with a minimal linewidth obtained for a slight negative detuning from the filter's central frequency, while a positive detuning frequency significantly increases the linewidth. To keep the laser linewidth constant during the chirp, the difference between the laser emission frequency and the filter central frequency must therefore be constant. The following section provides a detailed explanation of the chirp implementation.

3. FMCW performance

To achieve high-resolution DOFS measurement, the chirp amplitude of the laser is the key parameter. In a first step, we modulate only the SOA current and measure the frequency variation shown in Fig. 7, by using an unbalanced interferometer.

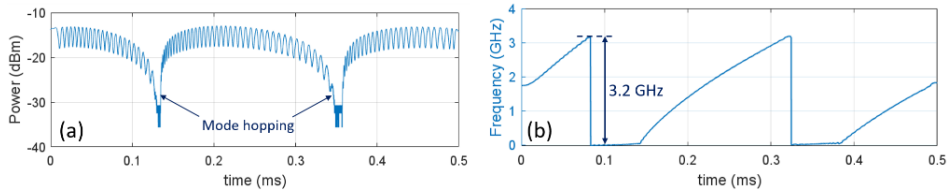

Fig. 7. (a) Time traces obtained at the output of the unbalanced interferometer. (b) Frequency vs. time curve with 500 MHz/mA modulation efficiency when only the gain section is modulated at a repetition rate of 1 kHz.

These measurements show that the mode-hop free laser frequency chirp through SOA current modulation only is limited to 3.2 GHz with a modulation efficiency of 500 MHz/mA, which corresponds to the cavity longitudinal mode spacing. A significant power variation following the shape of the Vernier filter reflection peak also occurs alongside frequency modulation. To solve these issues, we modulate the Vernier filter and the SOA simultaneously to keep the laser mode in the center of the Vernier filter. This prevents mode hopping and maintains a constant output power, as well as a constant linewidth, as discussed in previous section. As a result, we were

Optics EXPRESS

able to increase the chirp amplitude up to 20 GHz currently limited by the heating efficiency and driving electronics, as shown in Fig. 8.

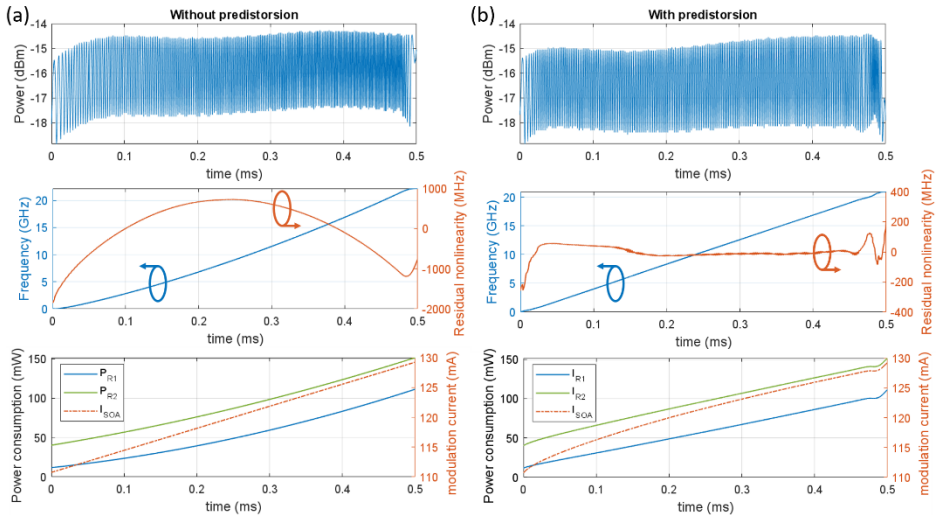

Fig. 8. Upper figures show the time traces obtained at the output of the unbalanced interferometer. Center figures show the laser frequency variation versus time (blue) with the corresponding residual nonlinearities (orange) before (a) and after (b) predistorsion of the modulation signals. Bottom figures display the power consumption of the ring heaters (left axis) and the SOA driving current (right axis) during the frequency tuning.

For tuning the filter central frequency, both resonators are tuned together through the thermo-optic effect. Compared to the piezoelectric effect, the rings are modulated more effectively, resulting in higher chirp amplitudes. However, this comes at the cost of limited frequency modulation waveform repetition rate, which cannot exceed 10 kHz, and significant nonlinearities. Figure 8(a) shows residual nonlinearities at approximately 10%, which can negatively impact DOFS measurement. They can cause significant differences in the beating electrical spectrum, leading to measurement inaccuracies [18]. To reduce this effect, we use an Arbitrary Waveform Generator (AWG) to generate predistorted signals to drive the laser (Fig. 8(b)). These signals are obtained through a process of iterative measurement of the chirp nonlinearity, followed by the implementation of corrective feedback on the modulation signals. The rate of nonlinearities is then reduced by an order of magnitude to less than 1% as shown in Fig. 8(b).

4. DOFS measurements

The laser is then integrated into a calibrated deformation field measurement setup [19] for DOFS measurements, shown in Fig. 9(a). The setup includes a FUT with a total length of 87 m. At 54 m from the fiber input there is a suspended metal plate with calibrated mechanical vibrational modes, on which the fiber is coiled over a length of 8.5 m, as shown in Fig. 9(b). A shaker is then used to excite the eigenmodes of the plate, which are perfectly known and simulated. Finally, the model established by Sirkis [20] enables us to correlate optical fiber deformations with the optical phase variations measured by the OFDR interrogator. Spurious effects such as optical polarization distortion start to occur at short bending radii of the fiber. For this reason, we only measure the RBS phase along the first half of the coiled fiber (see Fig. 10).

To extract the Rayleigh backscattered signal (RBS) phase variations from the beating signal time trace, we iterate the signal processing described in the introduction for each repetition of the laser chirp waveform. This gives the evolution of the RBS phase as a function of time for each

Optics EXPRESS

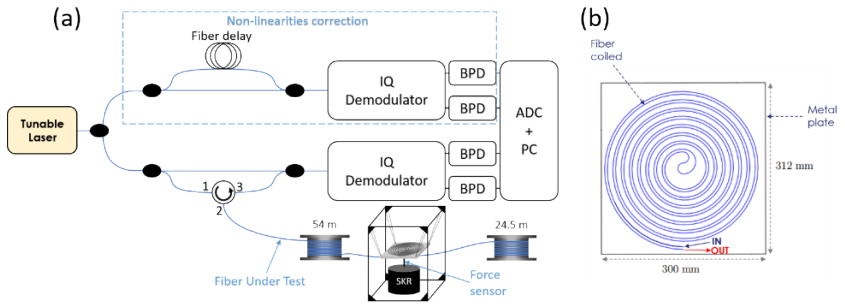

Fig. 9. (a) Schematic of the DOFS setup used, SKR: shaker. (b) Illustration of the fiber coiled on the metal plate.

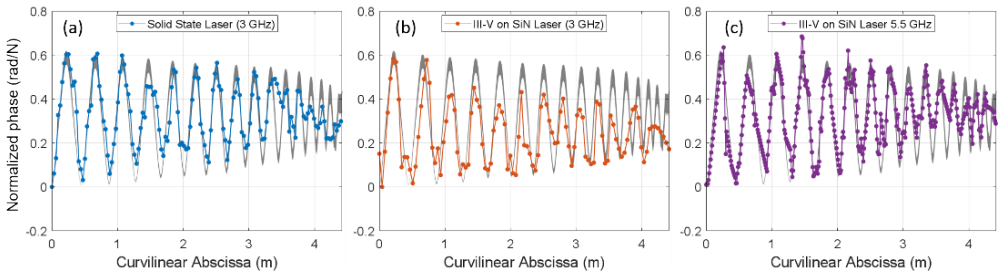

Fig. 10. Experimental DOFS measurements using different tunable laser sources. (a) Custom THALES RT solid state laser, (b) III-V-on-SiN laser with 3 GHz chirp amplitude, (c) high resolution measurement with III-V-on-SiN laser at 5.5 GHz chirp amplitude. The grey area shows the expected theoretical vibrational mode of the metal plate.

position in the FUT (Eq. (1)). Then, by performing a second FFT on this signal along the time axis, we can extract the amplitude of the phase variations that evolve at the frequency of interest (the frequency of the vibrational eigenmodes of the plate) and whose backscattering centers are at the position of interest (the plate position). We focus on the deformation of the optical fiber induced by the first plate's eigenmode at 484 Hz. Measurements are performed with two lasers, including the solid-state laser and the III-V-on-SiN laser. Figure 10 shows the measurements and the simulation of the accumulated optical phase (represented by the grey curve) as a function of the curvilinear abscissa at the location of the metal plate. The first laser (a) is a homemade solid state laser with a narrow linewidth <10 Hz [21], and the measurement was performed at its maximum chirp amplitude of 3 GHz with a 3 kHz repetition rate. For the III-V-on-SiN laser measurement, we use the higher linewidth laser (9.9 kHz) under two different chirp conditions: 3 GHz (b) and 5.5 GHz for extended spatial resolution (c), both with a 3 kHz repetition rate. The measurements at 3 GHz for the solid-state and III-V-on-SiN lasers give comparable results, close to the simulated phase response of the sensor. For the implemented fiber length of about 100 m, the 10 kHz linewidth of the III-V-on-SiN laser is low enough not to degrade noticeably the phase measurement signal-to-noise ratio (SNR). Moreover, with its higher chirp amplitude capability, our laser improves the spatial resolution of the sensor. As shown in Fig. 10(c) the distance between two backscattering centers is reduced. This improved resolution enables to better resolve sharp phase variation peaks. It can however be noticed in Fig. 10(a)-(c) that the fidelity of the measurement slightly degrades with distance along the fiber. This is attributed to polarization distortion effects occurring when bending radius of the coiled fiber becomes smaller in the center of the spiral.

Optics EXPRESS

5. Discussion

This work demonstrates the use of heterogeneous integration of III-V material on SiN to realize an FMCW laser source. The low losses of SiN allowed us to take advantage of high-quality micro-ring resonators, resulting in a frequency agile narrow linewidth laser (<10 kHz). The performances obtained with our integrated laser are comparable to those of bulk lasers currently on the DOFS market. We have also demonstrated that for the two lasers realized, the performance levels are in line with simulation. allowing us consider more complex designs. This laser building block is incorporated in a complete fully integrated OFDR interrogator which is currently being manufactured. The device includes the laser source, the calibration interferometer with a 1 m delay line, the on-chip recombination of the sensor interferometer and I/Q photodiodes for both interferometers. With a total size of 14.5×3.8 mm^2, the SWAP of the current interrogator will be drastically reduced. This reduction will enable the system's deployment into new and more constrained environments, expanding its field of application.

6. Conclusion

We have described a new type of laser made by heterogeneous integration of InP and SiN, combining low linewidth with high chirp capacity. The performances obtained meet the requirements of DOFS applications with a sub-cm spatial resolution. The laser's chirp amplitude exceeds 20 GHz (at a repetition rate of 1 kHz). Thanks to its design, which incorporates a double ring resonator mirror, we obtain a linewidth reduction factor close to 1000, resulting in a measured linewidth of 2.4 kHz. The preliminary OFDR measurements show performance comparable to other FMCW laser sources tested, and an improved spatial resolution. These results are very promising for the complete integration of the OFDR interrogator, currently in fabrication.

Funding. Association Nationale de la Recherche et de la Technologie; Horizon 2020 Framework Programme (101017088).

Disclosures. The authors declare no conflicts of interest.

Data availability. Data underlying the results presented in this paper may be obtained from the authors upon reasonable request.

References

1. A. Barrias, J. R. Casas, and S. Villalba, "A review of distributed optical fiber sensors for civil engineering applications," Sensors **16**(5), 748 (2016).
2. H. Wijaya, P. Rajeev, and E. Gad, "Distributed optical fibre sensor for infrastructure monitoring: Field applications," Opt. Fiber Technol. **64**, 102577 (2021).
3. M. R. Fernández-Ruiz, M. A. Soto, E. Williams, *et al.*, "Distributed acoustic sensing for seismic activity monitoring," APL Photonics **5**(3), 1 (2020).
4. A. Masoudi and T. P. Newson, "Contributed review: distributed optical fibre dynamic strain sensing," Rev. Sci. Instrum. **87**(1), 1 (2016).
5. C. Liang, Q. Bai, M. Yan, *et al.*, "A comprehensive study of optical frequency domain reflectometry," IEEE Access **9**, 41647–41668 (2021).
6. B. Behroozpour, P. A. M. Sandborn, M. C. Wu, *et al.*, "Lidar system architectures and circuits," IEEE Commun. Mag. **55**(10), 135–142 (2017).
7. G. Zhang, Z. Ding, K. Wang, *et al.*, "Demonstration of high output power DBR laser integrated with SOA for the FMCW LiDAR system," Opt. Express **30**(2), 2599 (2022).
8. G. Lihachev, A. Bancora, V. Snigirev, *et al.*, "Frequency agile photonic integrated external cavity laser," arXiv, (2023).
9. M. A. Tran, D. Huang, J. Guo, *et al.*, "Ring-resonator based widely-tunable narrow-linewidth SI/INP integrated lasers," IEEE J. Sel. Top. Quantum Electron. **26**(2), 1–14 (2020).
10. G. Lihachev, J. Riemensberger, W. Weng, *et al.*, "Ultralow-noise frequency-agile photonic integrated lasers," arXiv, (2021).
11. B. Pan, J. Bourderionnet, V. Billault, *et al.*, "III-V-on-silicon nitride narrow-linewidth tunable laser based on micro-transfer printing," *Optical Fiber Communication Conference (OFC)* 2023.
12. C. O. De Beeck, B. Haq, L. Elsinger, *et al.*, "Heterogeneous III-V on silicon nitride amplifiers and lasers via microtransfer printing," Optica **7**(5), 386 (2020).

Optics EXPRESS

13. B. Pan, J. Bourderionnet, V. Billault, *et al.*, " III-V-on-Si3N4 widely tunable narrow linewidth laser based on micro-transfer printing" Photon. Res. submitted for publication.
14. M. A. Tran, D. Huang, and J. E. Bowers, "Tutorial on narrow linewidth tunable semiconductor lasers using Si/III-V heterogeneous integration," APL Photonics **4**(11), 1 (2019).
15. J. E. Heebner, Optical Microresonators : Theory, Fabrication, and Applications (2007).
16. R. F. Kazarinov and C. H. Henry, "The relation of line narrowing and chirp reduction resulting from the coupling of a semiconductor laser to passive resonator," IEEE J. Quantum Electron. **23**(9), 1401–1409 (1987).
17. L.A. Coldren, S.W. Corzine, and M.L. Mashanovitch, "*Diode lasers and photonic integrated circuits*." John Wiley & Sons (2012).
18. S. Ayhan, S. Scherr, A. Bhutani, *et al.*, "Impact of frequency ramp nonlinearity, phase noise, and SNR on FMCW radar accuracy," IEEE Trans. Microwave Theory Tech. **64**(10), 3290–3301 (2016).
19. P. Charliac, C. Travers, I. Ghobrel, *et al.*, "Quantitative measurement of deformation fields by High Resolution Dynamic Optical OFDR System," *Optical Fiber Communication Conference (OFC)* 2023
20. J.S. Sirkis and H.W. Haslach, "Complete phase-strain model for structurally embedded interferometric optical fiber sensors," J. Intell. Mater. Syst. Struct. **2**(1), 3–24 (1991).
21. J. Maxin, G. Pillet, B. Steinhausser, *et al.*, "Widely tunable opto-electronic oscillator based on a dual-frequency laser," J. Lightwave Technol. **31**(17), 2919–2925 (2013).